CrystEngComm

Cite this: *CrystEngComm*, 2012, **14**, 2817

www.rsc.org/crystengcomm

PAPER

An unusual 3D metal–organic framework, $\{[Ag_4(\mu_4\text{-pzdc})_2(\mu\text{-en})_2]\cdot H_2O\}_n$: C–H···Ag, N–H···Ag and (O–H)···Ag interactions and an unprecedented coordination mode for pyrazine-2,3-dicarboxylate†

Okan Zafer Yeşilel,*[a] Güneş Günay,[a] Cihan Darcan,[b] Mustafa Serkan Soylu,[c] Seda Keskin[d] and Seik Weng Ng[e]

Received 29th November 2011, Accepted 4th January 2012
DOI: 10.1039/c2ce06603c

A novel three-dimensional (3D) metal–organic framework of silver(I)-pyrazine-2,3-dicarboxylate (pzdc) with ethylenediamine ligand (en), $\{[Ag_4(\mu_4\text{-pzdc})_2(\mu\text{-en})_2]\cdot H_2O\}_n$ (**1**), was synthesized and structurally characterized by spectral methods (FT-IR and photoluminescence), elemental analysis, thermal analysis (TG, DTG, DTA) and single crystal X-ray diffraction techniques. X-ray crystallographic study of **1** revealed that the pzdc ligand adopts a new coordination mode. Four Ag(I) atoms with different coordination geometries are linked together with carboxylate groups to form 1D tetranuclear building block. The adjacent 1D blocks are connected through the en ligand to form a 2D layer structure, which is further connected to a 3D framework by argentophilic interaction (Ag1···Ag2 = 3.096 and Ag3···Ag4 = 3.3070 Å). The complex exhibits C–H···Ag, N–H···Ag intermolecular multicenter heteroacceptor (IMH) hydrogen-bonding interactions between the Ag(I) ions and hydrogen atoms of the en ligand and (O–H)···Ag interaction of the pseudo-agostic (IPA) between the Ag(I) ion and hydrogen atoms of the water molecule. In order to assess the potential of **1** in gas storage applications, we performed atomically detailed simulations. Furthermore, **1** exhibits green and unusual yellow luminescence in the solid state at room temperature. Complex **1** has also good antimicrobial activity (36–63 μg mL^{-1}) on studied microorganisms.

Introduction

Recently, many coordination polymers have been designed and constructed due to their variety of intriguing topologies and their potential applications in areas such as magnetism, catalysis, gas storage and conductivity.[1,2] The selection of the ligand and metal ions is extremely important in the construction of these coordination polymers.[1] In addition to the choice of ligands and metal ions, reaction conditions such as solvents, pH, reacting time, and temperature can also affect the final structure.[3,4] Generally, the multidentate ligands are widely used as molecular building blocks in the construction of coordination polymers of high dimensionality.[5,6] Among these, benzene-based di- and multi-carboxylate ligands have been extensively studied because of the diversity of coordination modes and sensitivity to pH of the carboxylate groups.[7,8] In contrast, studies on heteroaromatic dicarboxylate ligands are far less common than the studies of benzenecarboxylates. Among them, pyrazine-2,3-dicarboxylate (pzdc) has proved to be an interesting and multifunctional ligand and it exhibits various coordination modes such as monodentate, bidentate, bis(bidentate) bridging and multidentate bridging.[9–12]

Non-covalent forces such as hydrogen bonding and π···π interactions, have been extensively used in supramolecular chemistry.[13,14] In addition to intra- or intermolecular interactions, the relatively weak interactions such as X–H···M close interactions (where X can be C, N or O and M = metal atom) often play crucial roles in supramolecular compounds.[15] To the best of our knowledge, only a few examples with X–H···Ag close interactions identified by X-ray diffraction have been reported.[16,17]

Many examples of polynuclear structures have been reported in the chemistry of silver carboxylate.[18,19] Although many coordination polymers constructed by the pyrazine-2,3-dicarboxylate ligand have been reported, most of them focused on transition metals such as Co(II), Cu(II), Zn(II) and Cd(II),[20–22] whereas those using Ag(I) are very rare, and only seven silver(I) complexes, $[Ag_2(pzdc)(H_2O)(hmt)]\cdot 2H_2O$,[23] $[Ag(NH_3)_2][Ag_3(pzdc)_2(NH_3)_4]$,[11] $[Ag_3(pzdc)(Hpzdc)]n$,[12] $[Ag_2(pzdc)]$,[24] $[Ag_2(pzdc)(H_2O)]$,[25] (NH_4)

[a]*Department of Chemistry, Faculty of Arts and Sciences, Eskişehir Osmangazi University, 26480 Eskişehir, Turkey. E-mail: yesilel@ogu.edu.tr; Fax: +90 222 2393578; Tel: +90 2222393750/ext. 2867*
[b]*Department of Biology, Faculty of Arts and Sciences, Dumlupınar University, 43100 Kütahya, Turkey*
[c]*Department of Physics, Faculty of Arts and Sciences, Giresun University, Giresun, Turkey*
[d]*Department of Chemical and Biological Engineering, Koç University, İstanbul, Turkey*
[e]*Department of Chemistry, University of Malaya, 50603 Kuala Lumpur, Malaysia and Department of Chemistry, Faculty of Science, King Abdulaziz University, PO Box 80203, Jeddah, Saudi Arabia and the Ministry of Higher Education of Malaysia, (grant No. UM.C/HIR/MOHE/SC/12)*
† CCDC reference number 823200. For crystallographic data in CIF or other electronic format see DOI: 10.1039/c2ce06603c

$[Ag(pzdc)]_n$[26] and $[Ag_2(bmimb)_{1.5}(pzdc)\cdot 3H_2O]_n$,[27] appeared in this field.

We have long been interested in the coordination chemistry of the pyrazine-2,3-dicarboxylate ligand since pzdc acts a versatile ligand and it may coordinate to metals by means of its pyrazine nitrogen and carboxyl oxygen atoms.[10,20,28] In this study, we present a new mixed-ligand 3D silver(I)-pyrazine-2,3-dicarboxyl ate coordination polymer with ethylenediamine (en), namely $\{[Ag_4(\mu_4\text{-pzdc})_2(\mu\text{-en})_2]\cdot H_2O\}_n$ (**1**).

Materials and measurements

All chemicals used were of analytical grade and were purchased commercially. The IR spectrum was obtained using a Perkin Elmer 100 FT-IR spectrometer using KBr pellets in the 4000–400 cm^{-1} range. A Perkin Elmer Diamond TG/DTA Thermal Analyzer was used to record simultaneous TG, DTG and DTA curves in a static air atmosphere at a heating rate of 10 °C min^{-1} in the temperature range 30–700 °C using platinum crucibles. The photoluminescence (excitation and emission) spectrum for the solid complex sample was determined with a Perkin-Elmer LS-55 spectrophotometer.

Synthesis of 1

A solution of $K_2[Cu(pzdc)_2(H_2O)]$[29] (0.500 g, 8.3 mmol) in water (20 mL) was added dropwise with stirring to a solution of $AgNO_3$ (0.280 g, 1.6 mmol) in water (20 mL). The mixture was stirred for 4 h at 50 °C and then en (0.074 g, 1.2 mmol) in water (25 ml) was added to the mixture to give a clear solution. The resulting solution was left to evaporate slowly in the dark at room temperature for several weeks to give pale yellow needle-like crystals of **1**. The crystals were washed with water and dried in air. Yield: 61.4% based on Ag. Elemental analysis for $C_{14}H_{14}AgN_6O_9$: Found: C, 20.15; H, 1.82; N, 9.83%. Calcd.: C, 19.98; H, 1.68; N, 9.98%. Selected IR peaks (cm^{-1}): 3416 (s), 3302 (w), 3242 (w), 2929 (w), 1608 (vs), 1585 (vs), 1431 (m), 1382 (m), 1350 (s), 1109 (m), 827 (m), 731 (m), 594 (w), 430 (w).

X-ray structure determination

Diffraction measurements were performed at 100 K on an Oxford Diffraction SuperNova diffractometer that was equipped with Mo radiation. The structures were solved by direct methods using the program SHELXS-97[30] with anisotropic thermal parameters for all non-hydrogen atoms. All non-hydrogen atoms were refined anisotropically by full-matrix least-squares methods using SHELXL-97.[30] Molecular drawings were obtained using Mercury.[31]

Details of the refinement are presented in Table 1; the crystallographic information file is deposited with the CCDC as 823200.

DFT computation and the natural bond orbital analysis

Single-crystal X-ray diffraction analysis reveals that the molecular packing of **1** has a 3D supramolecular framework and the asymmetric unit consists of four Ag(I) ions. Four Ag(I) ions exhibit four different coordination geometries. Considering the difficulty of doing quantum mechanical calculations and geometry optimization for such a large system, we started NBO analysis[32] from the X-ray geometry. The calculation was carried out using the Becke–3–Lee–Yang–Parr (B3LYP) exchange–correlation functional[33,34] in conjunction with a 3–21G basis set using a relativistic effective core potential for the metals[35,36] by the help of GAUSSIAN03 program.[37]

Table 1 Crystal data and structure refinement for **1**

Formula	$C_{14}H_{14}AgN_6O_9$
Formula weight	841.79
Crystal system	Triclinic
Space group	$P\bar{1}$
a (Å)	8.0419 (3)
b (Å)	8.3021 (4)
c (Å)	14.7143 (7)
α (°)	92.045 (4)
β (°)	97.070 (3)
γ (°)	95.305 (3)
V (Å^3)	969.65 (7)
Z	2
D_x (Mg m^{-3})	2.883
μ (mm^{-1})	4.05
F_{000}	800
T (K)	100
Crystal dimensions (mm)	0.25 × 0.20 × 0.15
Index range	$h = -10 \rightarrow 10$
	$k = -10 \rightarrow 10$
	$l = -19 \rightarrow 19$
Measured reflections	10 299
Independent reflections	4315
Reflections with $I > 2\sigma(I)$	3908
$R[F^2 > 2\sigma(F^2)]$	0.025
$wR(F^2)$	0.078
$(\Delta/\sigma)_{max}$	0.001
$\Delta\rho_{max}$ (e Å^{-3})	0.96
$\Delta\rho_{min}$ (e Å^{-3})	−0.82
S	1.13

Details of molecular simulations

In order to assess the potential of **1** in gas storage applications, we performed molecular simulations. Grand Canonical Monte Carlo (GCMC) simulations were used to compute adsorption of H_2 in **1**. A rigid and solvent-free structure of **1** was used in molecular simulations. The universal force field (UFF)[38] was used for the framework atoms. A number of studies in the past showed that several general-purpose force fields including UFF employed in adsorption simulations of metal organic frameworks (MOFs) give reasonable agreement with experiments.[39] Spherical Lennard-Jones (LJ) 12–6 potentials were used to model H_2.[40] This potential model has been successfully adopted in the past to predict adsorption behavior of H_2 in various MOFs.[41,42] Interactions between H_2 molecules and the atoms of **1** were modeled using pair-wise interactions between H_2 molecules and each atom in **1**. Mixed-atom interactions were defined using the Lorenz–Berthelot mixing rules. The interaction potential parameters used in the GCMC simulations for adsorbate (H_2) and MOF (**1**) atoms are given in Table 2. Parameters ε and σ represent the energy and size parameters of the LJ potential (U_{LJ}), whereas r is the distance between particles:

$$U_{LJ} = 4\varepsilon_{ij}\left[\left(\frac{\sigma_{ij}}{r_{ij}}\right)^{12} - \left(\frac{\sigma_{ij}}{r_{ij}}\right)^{6}\right] \quad (1)$$

Table 2 Interaction potential parameters for adsorbent and adsorbate atoms used in this work

Atom/molecule	ε/k_B (K)	σ (Å)
C	52.87	3.43
H	22.16	2.57
N	34.75	3.26
O	30.21	3.12
Ag	18.13	2.81
H_2	34.20	2.96

Antimicrobial activity tests

This study was used two gram (−) bacteria (*E. coli* ATCC25922, *P. aeruginosa* ATCC27853), two gram (+) bacteria (*B. cereus* ATCC7064, *S. aureus* ATCC64535) and a yeast (*C. albicans* ATCC10231) as microorganisms. The results were compared to pyrazine-2,3-dicarbocxylic acid. **1** and pyrazine-2,3-dicarboxylic acid were dissolved at 2.5 mg mL^{-1} stock concentration in water. Complex **1** was also dissolved in the form of a suspension in water and DMSO. Antimicrobial activity tests were carried out using the broth dilution method. The cultures were grown in 5 mL nutrient broth (Merck) at 37 °C for 18 h at 175 rpm in an orbital shaker incubator. Initial bacterial concentrations (approximately 5×10^5 cfu mL^{-1}) were estimated for the cultures by matching with 0.5 McFarland standards at 600 nm. **1** and H_2pzdc were tested in two-fold serial dilutions; eventually the ranges were narrowed to define more exact values. The minimum inhibitor concentration (MIC) value was determined as the lowest concentration at which the growth of bacteria was not observed.

Results and discussion

Crystal structure of $\{[Ag_4(\mu_4\text{-pzdc})_2(\mu\text{-en})_2]\cdot H_2O\}_n$ (1)

Single-crystal X-ray diffraction analysis reveals that **1** crystallizes in the triclinic space group $P\bar{1}$ and has a 3D framework. The asymmetric unit consists of four Ag(I) ions, two pzdc, two en ligands and one lattice water molecule. As shown in Fig. 1, four Ag(I) ions exhibit four different coordination geometries, in which the pzdc ligand displays an unprecedented μ_4-coordination mode (Scheme 1). Ag1 adopts a distorted square pyramidal geometry, which is coordinated by a carboxyl oxygen atom, one nitrogen atom from a pzdc ligand and one nitrogen atom from one en ligand. Ag2 is in a distorted trigonal pyramidal coordination environment, coordinated by three carboxyl oxygen atoms (O2, O3 and O4) from two different pzdc ligands and one nitrogen atom from the pzdc ligand (Ag2–N4 = 2.283 Å). The Ag3 ion is coordinated by one carboxyl oxygen and pyrazine nitrogen atom from one pzdc ligand and one nitrogen atom from an en ligand. The coordination environment of Ag3 can be described as T-shaped. Ag4 is also coordinated by four atoms in a distorted trigonal pyramidal geometry: two carboxyl oxygen atoms and one nitrogen atom from two different pzdc ligands in the equatorial position, and one oxygen atom from one pzdc ligand in the axial position. The Ag–O and Ag–N distances are in the range of 2.306(3)–2.707(3) Å and 2.153(3)–2.304(3) Å, respectively, which are similar to the reported Ag–O and Ag–N distances in other Ag(I)–pzdc complexes (Table 3).[11,23] Each pzdc ligand connects four Ag(I) ions through all of six donor atoms to form a 1D chain with a new coordination mode, which are further linked by en ligands to generate a 2D layer (Fig. 2). As shown in Fig. 3, the resulting 2D layers are extended into a 3D framework through strong Ag···Ag interactions. The Ag1···Ag2 and Ag3···Ag4 distances are 3.096 and 3.3070 Å, respectively, which are shorter than twice the van der Waals radii of Ag(I) (3.44 Å). This indicates ligand-unsupported Ag···Ag interactions. Thus, this interaction can be considered as d^{10}–d^{10} noncovalent bond (argentophilic interaction).[43,44] In **1**, the presence of an argentophilic interaction plays a vital role in the formation of the 3D coordination framework.

The most striking feature of **1** is the presence of obvious C–H···Ag, N–H···Ag intermolecular multicenter heteroacceptor (IMH) hydrogen-bonding interactions and (O–H)···Ag interaction of the pseudo-agostic (IPA) between the Ag ions and hydrogen atoms of the en ligand and water molecule

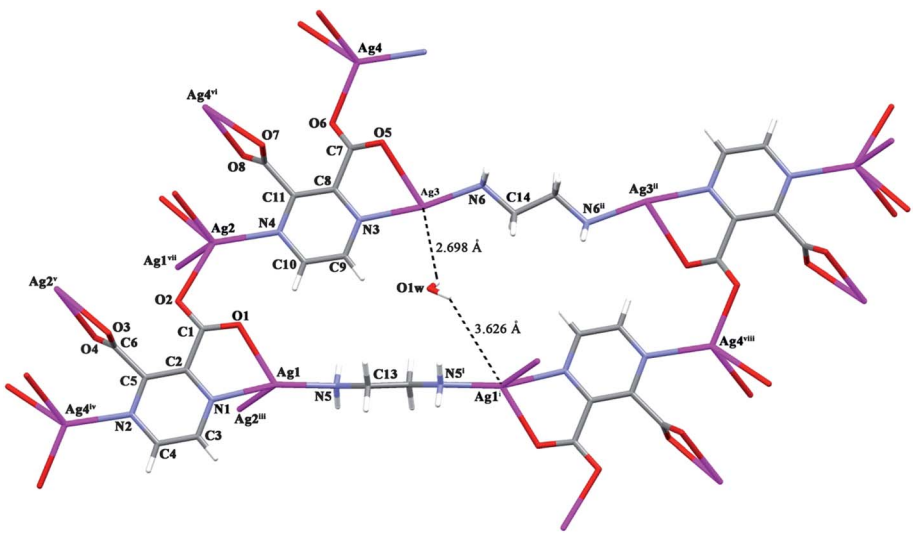

Fig. 1 The molecular structure of **1** showing the atom numbering scheme.

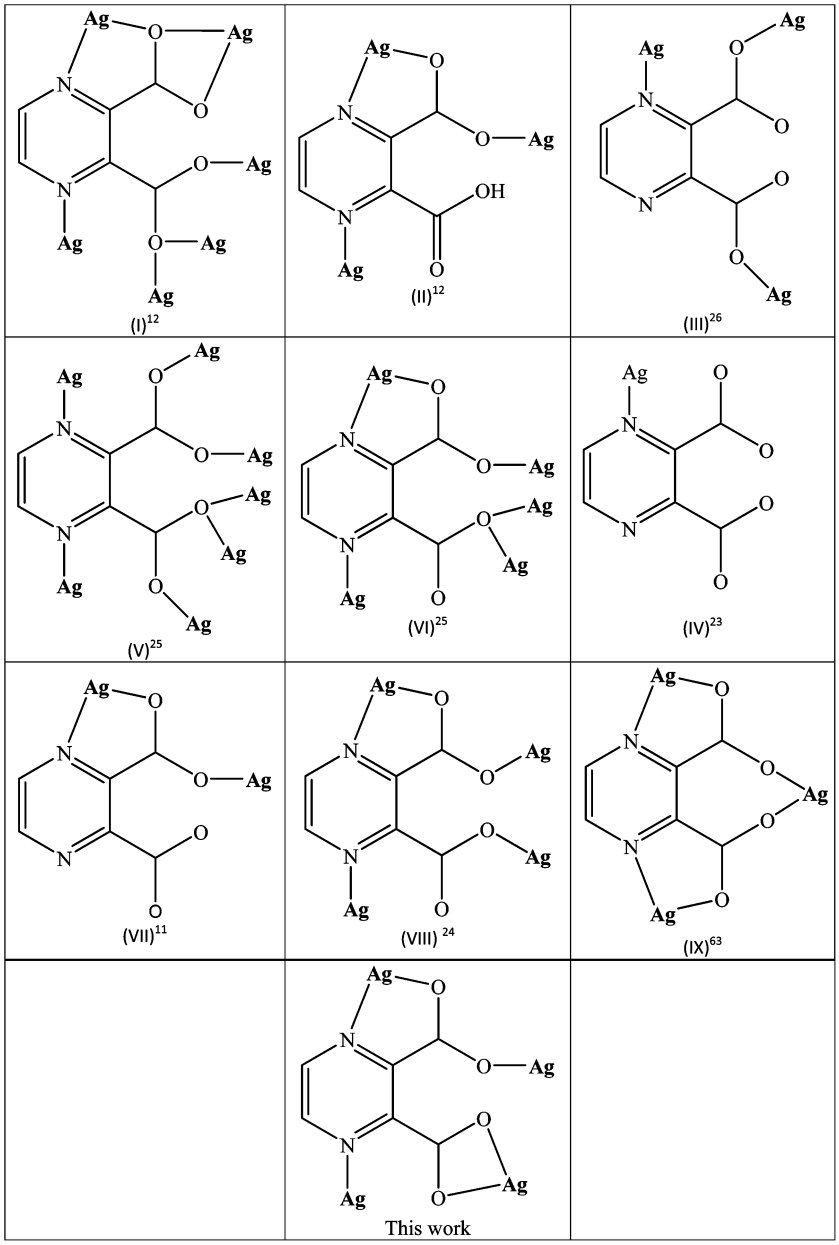

Scheme 1 Various possible coordination modes of the pzdc ligand with Ag atom.[11,12,23–26,63]

(Fig. 4 and Fig. 5.).[15] To the best of our knowledge, only a few examples of C–H···Ag close interactions identified by X-ray diffraction have been reported.[45,46] Furthermore, this complex is the first example including three C–H···Ag, N–H···Ag (IMH) and (O–H)···Ag (IPA) interactions. This weak hydrogen-bonding plays a crucial role in the architecture of the network polymers and biological systems.[47,48] So far, various X–H···Ag (X = C, N and O) close interactions have rarely been studied and reported.[15] The bond distances (Ag2···H13A and Ag2···C13) and angle (C13–H13A···Ag2) are 2.776 Å, 3.384 Å [d(Ag···H) < d(Ag···C)] and 121.03° [C–H···Ag > 100°], respectively. The Ag2···H52 and Ag2···N5 bond distances and N5–H52···Ag2 angle are 3.074 Å, 3.650 Å [d(Ag···H) < d(Ag···N)] and 125.17° [N–H···Ag > 100°], respectively. This kind of interaction in **1** should be well described as a weak intermolecular C(N)–H···M hydrogen-bonding interaction.[15] The bond distances (Ag3···H1W2 and Ag3···O1W) and angle (O1W–H1W2···Ag3) are 2.698 Å, 2.805 Å [d(Ag···H) ≈ d(Ag···O)] and 88.48° [O1W–H1W2···Ag3 < 100°], respectively. This type of interaction should be named as an *interaction of the pseudo-agostic* (IPA).[15]

Moreover, there are intermolecular Ag···π stacking interactions between Ag ions and the pyrazine ring (Fig. 4 and Fig. 5). The Ag–C bond distances in range from 3.266 to 3.816 Å, which are all within the normal range generally found the literature.[49,50] The Ag3–C3 and Ag3–C4 bond lengths are 3.391 and 3.266 Å, respectively. These lengths are shorter than the sum of the van der Waals radii of Ag and C (3.42 Å). These interactions in **1** may be considered as a medium dihapto aromatic coordination of the pyrazine ring to the Ag(I) ions. In addition, hydrogen bonds and π···π interactions also coexist in **1**. The N–H···O and strong O–H···O hydrogen bonds between nitrogen atoms of the en ligand and carboxyl oxygen atoms (N5···O4 = 2.928(4),

Table 3 Selected bond lengths (Å) and angles (°) for **1**[a]

Bond lengths			
Ag1–N1	2.229 (3)	Ag1–Ag2$^{a_{iv}}$	3.0955 (4)
Ag1–N5	2.153 (3)	Ag2–Ag1$^{a_{iv}}$	3.0955 (4)
Ag1–O1	2.426 (3)	Ag3–Ag4$^{a_{v}}$	3.3070 (4)
Ag2–N4	2.282 (3)	Ag4–Ag3$^{a_{v}}$	3.3070 (4)
Ag2–O2	2.337 (2)	Ag1–C1	3.6241
Ag2–O3$^{a_{i}}$	2.412 (3)	Ag1–C9	3.5452
Ag2–O4$^{a_{i}}$	2.592 (3)	Ag1–C10	3.4621
Ag3–N3	2.198 (3)	Ag2–C2	3.7740
Ag3–N6	2.158 (3)	Ag2–C3	3.4160
Ag3–O5	2.707 (3)	Ag2–C13	3.3846
Ag3–O1w	2.805 (3)	Ag3–C3	3.3905
Ag4–N2$^{a_{ii}}$	2.304 (3)	Ag3–C4	3.2663
Ag4–O6	2.306 (3)	Ag4–C8	3.5500
Ag4–O7$^{a_{iii}}$	2.415 (3)	Ag4–C14	3.6827
Ag4–O8$^{a_{iii}}$	2.592 (3)		
Bond angles			
N5–Ag1–N1	163.35 (11)	N3–Ag3–O5	69.24 (9)
N5–Ag1–O1	123.65 (10)	N6–Ag3–O1w	105.49 (10)
N1–Ag1–O1	71.43 (10)	N3–Ag3–O1w	83.11 (10)
N5–Ag1–Ag2$^{a_{iv}}$	98.60 (8)	O5–Ag3–O1w	146.28 (8)
N1–Ag1–Ag2$^{a_{iv}}$	69.76 (8)	N6–Ag3–Ag4$^{a_{v}}$	114.44 (9)
O1–Ag1–Ag2$^{a_{iv}}$	100.36 (7)	N3–Ag3–Ag4$^{a_{v}}$	68.66 (8)
N4–Ag2–O2	129.98 (10)	O5–Ag3–Ag4$^{a_{v}}$	103.78 (6)
N4–Ag2–O3$^{a_{i}}$	130.68 (9)	O1w–Ag3–Ag4$^{a_{v}}$	82.60 (6)
O2–Ag2–O3$^{a_{i}}$	98.78 (9)	N2$^{a_{ii}}$–Ag4–O6	121.69 (10)
N4–Ag2–O4$^{a_{i}}$	108.80 (9)	N2$^{a_{ii}}$–Ag4–O7$^{a_{iii}}$	137.60 (10)
O2–Ag2–O4$^{a_{i}}$	106.98 (9)	O6–Ag4–O7$^{a_{iii}}$	97.68 (9)
O3$^{a_{i}}$–Ag2–O4$^{a_{i}}$	53.01 (8)	N2$^{a_{ii}}$–Ag4–O8$^{a_{iii}}$	109.85 (9)
N4–Ag2–Ag1$^{a_{iv}}$	122.44 (8)	O6–Ag4–O8$^{a_{iii}}$	120.22 (9)
O2–Ag2–Ag1$^{a_{iv}}$	63.89 (6)	O7$^{a_{iii}}$–Ag4–O8$^{a_{iii}}$	52.92 (8)
O3$^{a_{i}}$–Ag2–Ag1$^{a_{iv}}$	68.21 (6)	N2$^{a_{ii}}$–Ag4–Ag3$^{a_{v}}$	118.92 (8)
O4$^{a_{i}}$–Ag2–Ag1$^{a_{iv}}$	118.80 (6)	O6–Ag4–Ag3$^{a_{v}}$	59.83 (7)
N6–Ag3–N3	171.02 (11)	O7$^{a_{iii}}$–Ag4–Ag3$^{a_{v}}$	65.79 (6)
N6–Ag3–O5	101.79 (10)	O8$^{a_{iii}}$–Ag4–Ag3$^{a_{v}}$	118.47 (6)

[a] Symmetry codes: (i) $-x+2, -y, -z+1$; (ii) $x-1, y, z-1$; (iii) $-x+1, -y, -z$; (iv) $-x+2, -y+1, -z+1$; (v) $-x+1, -y+1, -z$.

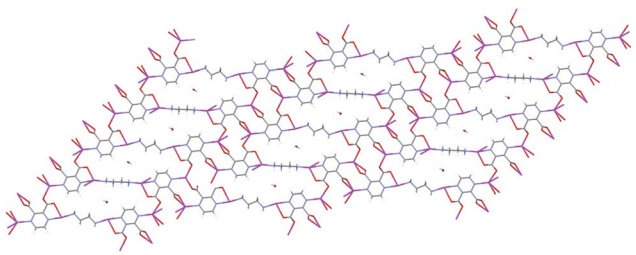

Fig. 2 An infinite 2D layer in **1**.

N6···O5 = 2.997(4) and N6···O8 = 2.954(4) Å) and oxygen atom of water molecule and carboxyl oxygen atoms (O1···O3 = 2.742(4) and O1···O7 = 2.720(4) Å) were found within the 3D framework (Table 4.). The shortest contact distance between the centroid of neighbouring pyrazine rings is 3.612(4) Å, which is suggestive of the weak π···π interaction.

Fluorescence spectrum

We also investigated the photoluminescent property of complex **1**. The free ligand H_2pzdc displays photoluminescence with

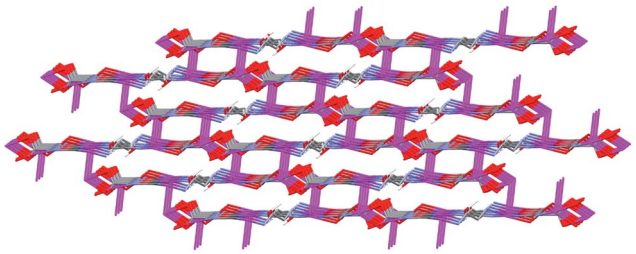

Fig. 3 The 3D metal–organic framework of **1** formed through Ag···Ag argentophilic interaction.

emission maxima at 390 nm (λ_{ex} = 388 nm). It can be presumed that this peak originate from the $\pi^* \rightarrow$ n or $\pi^* \rightarrow \pi$ transition. The fluorescence spectrum for **1** in the solid-state has been measured at room temperature and emission spectrum of **1** is shown in Fig. 6. It can be seen that complex **1** exhibits green and unusual yellow radiation emission maxima at *ca.* 530 nm and 580 nm upon photoexcitation at 385 nm. The emission may be assigned to the ligand-to-metal charge-transfer bands (LMCT).

Thermal decomposition

The thermal behavior of **1** was studied by TG and DTA in an air atmosphere in the temperature range of 30–1000 °C. The complex **1** shows a four step mass loss. The first stage between 133 and 234 °C corresponds to the endothermic elimination of one water molecule with a mass loss of 2.09% (calcd. 2.13%). The following stages in the temperature range of 234–357 °C correspond to the exothermic removal of the en and pzdc ligands with DTA peaks at 258, 311 and 353 °C (mass loss: found 45.23%, calcd. 46.60%). The final decomposition product of **1** is metallic silver.

Natural bond orbital analysis

Single-crystal X-ray diffraction analysis reveals that molecular packing of **1** has a 3D framework. The asymmetric unit consists of four Ag(I) ions and these Ag(I) ions exhibit four different coordination geometries, in which the pzdc ligand displays an unprecedented μ_4-coordination mode (Scheme 1). Therefore, it is important to investigate coordination around each of metal centers and delocalization effects to the coordination environments of the metal centers.

To investigate significant delocalization effects to the coordination environments of the metal atoms, the energetic stabilization due to the interactions between donor and acceptor pairs was estimated by second order perturbation theory analysis of the Fock matrix in natural bond orbital (NBO) basis carried out by SPE calculation at the optimized geometry. For each donor NBO (*i*) and acceptor NBO (*j*), the stabilization energy associated with delocalization between donor and acceptor is explicitly estimated by Eqn (2).[51]

$$E = \Delta E_{ij} = q_i \frac{F^2(i,j)}{\varepsilon_j - \varepsilon_i} \quad (2)$$

Where q_i is the *i*th donor orbital occupancy, ε_i and ε_j are diagonal elements (orbital energies) and $F(i,j)$ is the off diagonal element associated with the Fock matrix. Selected interactions that give

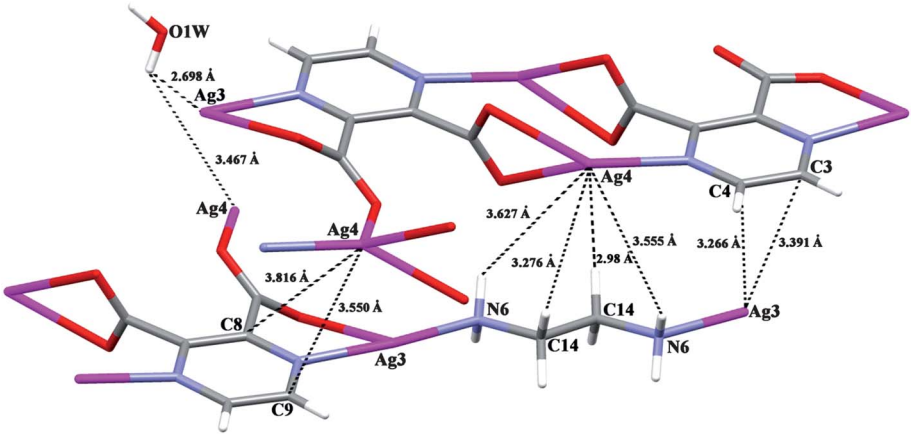

Fig. 4 The intra- and inter-molecular C–H···Ag, N–H···Ag, (O–H)···Ag and Ag···C interactions in **1**.

the strongest stabilization energies are given in Table 5. The interaction energy between carboxylate oxygens, pzdc nitrogens, en nitrogens and silver(I) center are also associated with corresponding distance among them. A decrease in the distances between donor atoms and acceptor center atoms is accompanied by the increment in the stabilization energy and determined by the estimation. For example, pzdc ligand acts as μ_2-ligand with one oxygen atom of carboxylate group and adjacent pyrazine nitrogen atom bridging Ag1 and Ag3 atoms through a five membered chelating mode. Among these binding modes, the longest O5–Ag3 distance of 2.707 Å gives the lowest stabilization energy to the structure. As shown in Table 5, the largest binding energies are in the nitrogen–metal interactions and therefore all the N–Ag distances are longer than O–Ag interactions.

Each pzdc ligand connects four Ag(I) ions to form 1D chain, which are further linked by en ligands to generate a 2D layer. The resulting 2D layers are extended into a 3D framework through strong Ag···Ag interactions. The Ag1···Ag2 and Ag3···Ag4 distances are 3.096 and 3.3070 Å, respectively, and indicate ligand-unsupported Ag···Ag interactions called argentophilic interactions.[43,52] These interactions were also revealed by the calculation and constituted stabilization energies of 1.74 and 2.36 kcal mol^{-1}, respectively, in the structure, as shown in the Table 5. The presence of this type of interaction plays a vital role in the formation of the 3D coordination framework.

Results of molecular simulations

Conventional GCMC simulations were employed to compute single component adsorption isotherms of H_2 at 77, 87 and 298 K. By specifying the temperature and fugacity of the adsorbing gases, the number of adsorbed molecules was calculated at equilibrium. Details of GCMC can be found elsewhere.[53] For pure components, four types of trial moves, attempts to translate a molecule, attempts to rotate a molecule, attempts to create a new molecule, and attempts to delete an existing molecule were included. A cut-off distance of 13 Å was used for LJ interactions. The interactions with **1** were pretabulated on a 0.2 Å grid. During

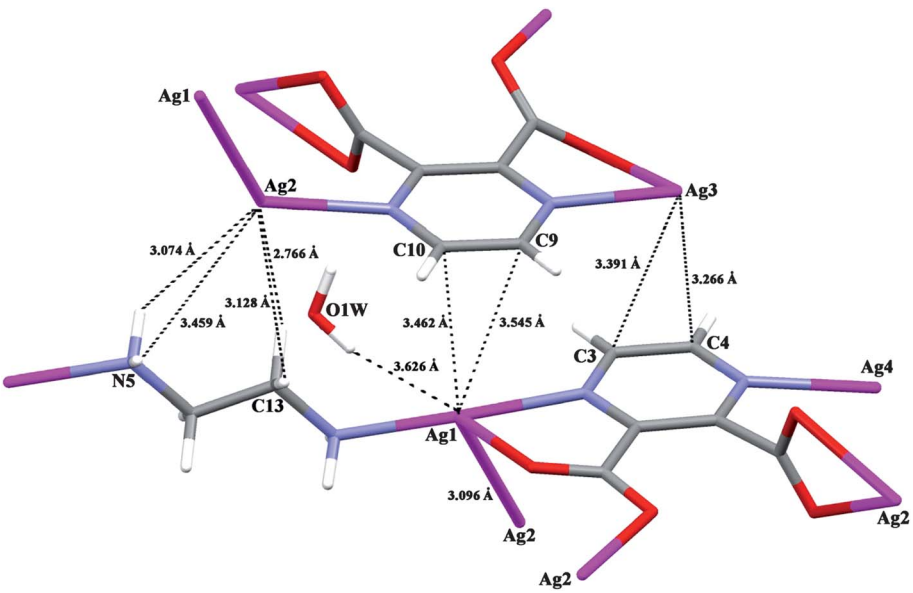

Fig. 5 The intra- and inter-molecular C–H···Ag, N–H···Ag, Ag···C and Ag···Ag interactions in **1**.

Table 4 Hydrogen bonding geometry (Å, °) for **1**[a]

D–H···A	D–H	H···A	D···A	D–H···A
N5–H52···O4$^{a_{iv}}$	0.88 (3)	2.08 (3)	2.928 (4)	164 (4)
N6–H62···O5$^{a_{ix}}$	0.88 (3)	2.12 (3)	2.997 (4)	172 (4)
N6–H61···O8$^{a_{v}}$	0.88 (3)	2.08 (3)	2.954 (4)	173 (4)
O1w–H1w1···O3$^{a_{x}}$	0.84 (3)	1.91 (3)	2.742 (4)	172 (5)
O1w–H1w2···O7$^{a_{xi}}$	0.84 (3)	1.89 (3)	2.720 (4)	171 (5)
X–H···Ag	**X–H**	**H···Ag**	**X···Ag**	**X–H···Ag**
C13–H13A···Ag2	0.990	2.77	3.384	121
C14–H14B···Ag4	0.990	2.97	3.683	129
C13–H13B···Ag2	0.989	3.13	3.384	96
C14–H14A···Ag4	0.990	3.28	3.847	118
O1w–H1w2···Ag3	0.845	2.69	2.805	88
O1w–H1w1···Ag3	0.844	3.25	2.805	52
O1w–H1w1···Ag1	0.844	3.63	4.140	122
N5–H52···Ag2	0.877	3.07	3.650	125

[a] Symmetry codes: (iv) −x + 2, −y + 1, −z + 1; (v) −x + 1, −y + 1, −z; (ix) −x, −y + 1, −z; (x) −x + 1, −y + 1, −z + 1; (xi) x, y + 1, z.

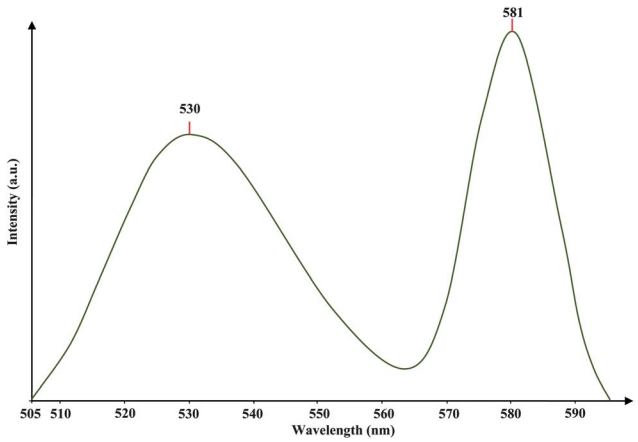

Fig. 6 The solid-state emission spectrum of **1** at room temperature.

Table 5 Second order perturbation theory analysis of the Fock matrix in NBO basis[a]

Donor	Acceptor	E^2 (kcal mol^{-1})	Bond length
O5 (LP)	Ag3 (LP*)	3.23	2.707
N3 (LP)	Ag3 (LP*)	45.67	2.198
N6 (LP)	Ag3 (LP*)	49.03	2.158
O1 (LP)	Ag1 (LP*)	7.77	2.426
N1 (LP)	Ag1 (LP*)	41.04	2.229
N5 (LP)	Ag1 (LP*)	47.36	2.153
O2 (LP)	Ag2 (LP*)	9.52	2.337
O3 (LP)	Ag2 (LP*)	5.08	2.412
O4 (LP)	Ag2 (LP*)	3.88	2.592
N4 (LP)	Ag2 (LP*)	13.16	2.283
O6 (LP)	Ag4 (LP*)	6.69	2.306
O7 (LP)	Ag4 (LP*)	5.20	2.415
O8 (LP)	Ag4 (LP*)	3.37	2.592
N2 (LP)	Ag4 (LP*)	6.21	2.306
Ag1 (LP)	Ag2 (LP*)	1.74	3.096
Ag3 (LP)	Ag4 (LP*)	2.36	3.307

[a] LP: a lone pair valence orbital and LP*: empty valence orbital NBOs.

the simulations, a 3D cubic Hermite polynomial interpolation scheme was used to calculate the potential at each point in space.[54] Periodic boundary conditions were applied in all simulations. The size of the simulation box was set to 2 × 2 × 2 crystallographic unit cells. Simulations at the lowest fugacity for each system were started from an empty **1** matrix and each subsequent simulation at higher fugacity was started from the final configuration of the previous run. Simulations included a minimum 1.5 × 10^7 cycle equilibration period followed by a 1.5 × 10^7 cycle production run.

Since **1** has a small pore volume, it exhibits low H_2 uptake. As the temperature is decreased, H_2 adsorption increases in **1** as expected. At 298 K, adsorption of H_2 in the pores of **1** is very limited. At 77 and 87 K, adsorption of H_2 reaches saturation at around 2 molecules H_2 per unit cell of **1** (Fig. 7).

Fig. 7 compares room temperature H_2 adsorption capacity of **1** with one of the well-known MOFs, IRMOF-1(MOF-5). The hydrogen adsorption capacity of IRMOF-1 is higher than the capacity of **1** under the same pressure conditions since IRMOF-1 has a very large pore volume compared to **1**.

Antimicrobial activity

The results are presented in Table 6 as MIC values (μg mL^{-1}), which is the minimum concentration to inhibit the growth of bacteria or yeast. The MIC values indicate that the antimicrobial activity of **1** was in the range of 18–63 μg mL^{-1} in the studied microorganisms. While pyrazine-2,3-dicarboxylic acid showed activity at higher concentrations on studied microorganisms (625 μg mL^{-1}), antimicrobial activity of **1** was greater than that of H_2pzdc. It is shown that the effectiveness of **1** was same for gram (−), gram (+) and eukaryotes. There is no significant difference among antimicrobial activities of **1** dissolved in different solvents.

The biological effect of various pzdc metal complexes was demonstrated in different studies.[10,55,56] It was reported that

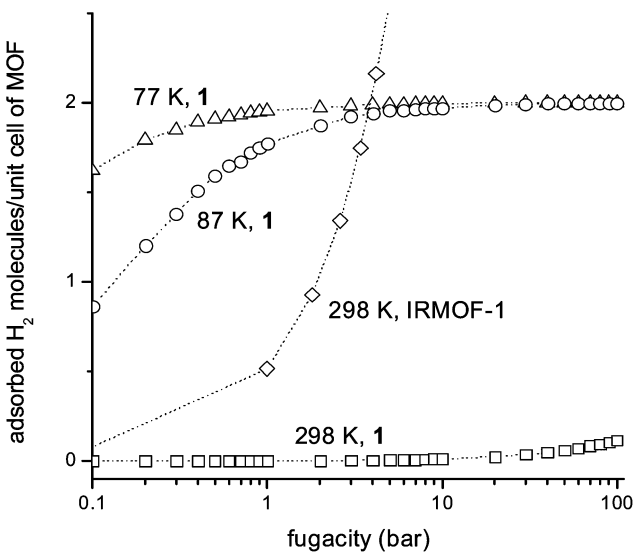

Fig. 7 H_2 adsorption isotherms in **1** at 77, 87 and 298 K computed from GCMC simulations as a function of pressure. H_2 adsorption isotherm of IRMOF-1 at 298 K is also given for comparison.

Table 6 The MICs of complex **1** (μg mL^{-1})

Compounds	Gram (−)		Gram (+)		Eukaryote
	E. coli	*P. aeruginosa*	*S. aureus*	*B. cereus*	*C. albicans*
1[a]	36	63	36	63	36
1[b]	36	63	18	36	36
Pyrazine-2,3-dicarboxylic acid[b]	625	625	625	625	625

[a] Dissolved in DMSO. [b] Dissolved in pure water.

pyrazine-2,3-dicarboxylic acid derivatives have strong antimicrobial activity against *Mycobacterium tuberculosis*.[57] Also, Ag alone has been demonstrated to possess antiviral, antibacterial and antifungal properties, and is also effective against other eukaryotic microorganisms.[58–60] Silver compounds are used as antimicrobial agents in many applications in medicine.[61,62] The complex **1** possesses good microbial activity.

Conclusions

In summary, an unusual 3D silver coordination polymer was successfully synthesized. The complex exhibits C–H···Ag, N–H···Ag intermolecular multicenter heteroacceptor (IMH) hydrogen-bonding interactions between the Ag ions and hydrogen atoms of an en ligand and (O–H)···Ag interaction of the pseudo-agostic (IPA) between the Ag ion and hydrogen atoms of water molecule. **1** exhibits strong green–yellow emission at room temperature, suggesting that **1** may be an efficient solid emitting material. Furthermore, the pzdc ligand exhibits a newly observed coordination mode compared to all previously reported compounds with the pzdc ligand.

Acknowledgements

This work has been supported by the Scientific and Technological Research Council of Turkey (TUBITAK, Project No: 109T201).

References

1 S. Kitagawa and R. Matsuda, *Coord. Chem. Rev.*, 2007, **251**, 2490–2509.
2 O. M. Yaghi, H. L. Li, C. Davis and T. Groy, *Abstr. Pap. Am. Chem. S.*, 1996, **212**, 250-INOR.
3 Y. Y. Yang, W. Guo and M. Du, *Inorg. Chem. Commun.*, 2010, **13**, 1195–1198.
4 L. S. Long, *CrystEngComm*, 2010, **12**, 1354–1365.
5 T. K. Maji and S. Kitagawa, *Pure Appl. Chem.*, 2007, **79**, 2155–2177.
6 S. Kitagawa, R. Kitaura and S. Noro, *Angew. Chem., Int. Ed.*, 2004, **43**, 2334–2375.
7 M. Liu, Z. P. Yang, W. H. Sun, X. P. Li, J. Li, J. S. Ma and G. Q. Yang, *Inorg. Chim. Acta*, 2009, **362**, 2884–2889.
8 Z. X. Li, X. Chu, G. H. Cui, Y. Liu, L. Li and G. L. Xue, *CrystEngComm*, 2011, **13**, 1984–1989.
9 M. Kondo, T. Okubo, A. Asami, S. Noro, T. Yoshitomi, S. Kitagawa, T. Ishii, H. Matsuzaka and K. Seki, *Angew. Chem., Int. Ed.*, 1999, **38**, 140–143.
10 O. Z. Yesilel, A. Mutlu, C. Darcan and O. Buyukgungor, *J. Mol. Struct.*, 2010, **964**, 39–46.
11 D. Sun, G. G. Luo, N. Zhang, Z. H. Wei, C. F. Yang, R. B. Huang and L. S. Zheng, *Chem. Lett.*, 2010, **39**, 190–191.
12 J. Wu, *Acta Crystallogr., Sect. C: Cryst. Struct. Commun.*, 2009, **65**, M91–M93.
13 L. Brammer, M. D. Burgard, M. D. Eddleston, C. S. Rodger, N. P. Rath and H. Adams, *CrystEngComm*, 2002, **4**, 239–248.
14 Q. G. Meng, S. T. Yan, G. Q. Kong, X. L. Yang and C. D. Wu, *CrystEngComm*, 2010, **12**, 688–690.
15 D. Braga, F. Grepioni, E. Tedesco, K. Biradha and G. R. Desiraju, *Organometallics*, 1997, **16**, 1846–1856.
16 X. B. Wang, J. Z. Feng, J. Huang, J. Y. Zhang, M. Pan and C. Y. Su, *CrystEngComm*, 2010, **12**, 725–729.
17 A. Ilie, C. I. Rat, S. Scheutzow, C. Kiske, K. Lux, T. M. Klapotke, C. Silvestru and K. Karaghiosoff, *Inorg. Chem.*, 2011, **50**, 2675–2684.
18 D. Sun, G. G. Luo, N. Zhang, Q. J. Xu, R. B. Huang and L. S. Zheng, *Polyhedron*, 2010, **29**, 1243–1250.
19 C. J. Wang, Y. Y. Wang, H. Wang, G. P. Yang, G. L. Wen, M. Zhang and Q. Z. Shi, *Inorg. Chem. Commun.*, 2008, **11**, 843–846.
20 O. Z. Yesilel, A. Mutlu and O. Buyukgungor, *Polyhedron*, 2008, **27**, 2471–2477.
21 H. Yin and S. X. Liu, *Polyhedron*, 2007, **26**, 3103–3111.
22 R. Kitaura, K. Fujimoto, S. Noro, M. Kondo and S. Kitagawa, *Angew. Chem., Int. Ed.*, 2002, **41**, 133–135.
23 G. Y. Wang, Z. Ma, B. Liu and C. Y. Cao, *Z. Krist.–New Cryst. St.*, 2010, **225**, 771–772.
24 F. Jaber, F. Charbonnier and R. Faure, *J. Chem. Crystallogr.*, 1994, **24**, 681–684.
25 J. H. Yang, S. L. Zheng, X. L. Yu and X. M. Chen, *Cryst. Growth Des.*, 2004, **4**, 831–836.
26 G. Smith, A. N. Reddy, K. A. Byriel and C. H. L. Kennard, *J. Chem. Soc., Dalton Trans.*, 1995, 3565–3570.
27 Fu-Jing Liu, Di Sun, Hong-Jun Haoa, Rong-Bin Huang and L.-S. Zheng, *CrystEngComm*, 2012, **14**, 379–382.
28 O. Z. Yesilel, G. Gunay, A. Mutlu, H. Olmez and O. Buyukgungor, *Inorg. Chem. Commun.*, 2010, **13**, 1173–1177.
29 O. Castillo, G. Beobide, A. Luque and P. Roman, *Acta Crystallogr., Sect. E: Struct. Rep. Online*, 2003, **59**, M800–M802.
30 G. M. Sheldrick, *SHELXS-97, Program for solution of crystal structures*, University of Göttingen, Germany, 1997; G. M. Sheldrick, *SHELXL-97, Program for refinement of crystal structures*, University of Göttingen, Germany, 1997.
31 C. F. Macrae, P. R. Edgington, P. McCabe, E. Pidcock, G. P. Shields, R. Taylor, M. Towler and J. van De Streek, *J. Appl. Crystallogr.*, 2006, **39**, 453–457.
32 A. E. Reed, L. A. Curtiss and F. Weinhold, *Chem. Rev.*, 1988, **88**, 899–926.
33 A. D. Becke, *J. Chem. Phys.*, 1993, **98**, 5648–5652.
34 C. T. Lee, W. T. Yang and R. G. Parr, *Phys. Rev. B*, 1988, **37**, 785–789.
35 P. J. Hay and W. R. Wadt, *J. Chem. Phys.*, 1985, **82**, 270–283.
36 A. W. Ehlers, M. Bohme, S. Dapprich, A. Gobbi, A. Hollwarth, V. Jonas, K. F. Kohler, R. Stegmann, A. Veldkamp and G. Frenking, *Chem. Phys. Lett.*, 1993, **208**, 111–114.
37 M. J. Frisch, G. W. Trucks, H. B. Schlegel, G. E. Scuseria, M. A. Robb, J. R. Cheeseman, J. A. Montgomery, Jr., T. Vreven, K. N. Kudin, J. C. Burant, J. M. Millam, S. S. Iyengar, J. Tomasi, V. Barone, B. Mennucci, M. Cossi, G. Scalmani, N. Rega, G. A. Petersson, H. Nakatsuji, M. Hada, M. Ehara, K. Toyota, R. Fukuda, J. Hasegawa, M. Ishida, T. Nakajima, Y. Honda, O. Kitao, H. Nakai, M. Klene, X. Li, J. E. Knox, H. P. Hratchian, J. B. Cross, V. Bakken, C. Adamo, J. Jaramillo, R. Gomperts, R. E. Stratmann, O. Yazyev, A. J. Austin, R. Cammi, C. Pomelli, J. Ochterski, P. Y. Ayala, K. Morokuma, G. A. Voth, P. Salvador, J. J. Dannenberg, V. G. Zakrzewski, S. Dapprich, A. D. Daniels, M. C. Strain, O. Farkas, D. K. Malick, A. D. Rabuck,

K. Raghavachari, J. B. Foresman, J. V. Ortiz, Q. Cui, A. G. Baboul, S. Clifford, J. Cioslowski, B. B. Stefanov, G. Liu, A. Liashenko, P. Piskorz, I. Komaromi, R. L. Martin, D. J. Fox, T. Keith, M. A. Al-Laham, C. Y. Peng, A. Nanayakkara, M. Challacombe, P. M. W. Gill, B. G. Johnson, W. Chen, M. W. Wong, C. Gonzalez and J. A. Pople, *GAUSSIAN 03 (Revision D.01)*, Gaussian, Inc., Wallingford, CT, 2004.
38 A. K. Rappe, C. J. Casewit, K. S. Colwell, W. A. Goddard and W. M. Skiff, *J. Am. Chem. Soc.*, 1992, **114**, 10024.
39 S. Keskin, J. Liu, R. B. Rankin, J. K. Johnson and D. S. Sholl, *Ind. Eng. Chem. Res.*, 2009, **48**, 2355–2371.
40 V. Buch, *J. Chem. Phys.*, 1994, **100**, 7610–7629.
41 A. I. Skoulidas and D. S. Sholl, *J. Phys. Chem. B*, 2005, **109**, 15760–15768.
42 G. Garberoglio, A. I. Skoulidas and J. K. Johnson, *J. Phys. Chem. B*, 2005, **109**, 13094–13103.
43 G. P. Yang, J. H. Zhou, Y. Y. Wang, P. Liu, C. C. Shi, A. Y. Fu and Q. Z. Shi, *CrystEngComm*, 2011, **13**, 33–35.
44 A. Serpe, F. Artizzu, L. Marchio, M. L. Mercuri, L. Pilia and P. Deplano, *Cryst. Growth Des.*, 2011, **11**, 1278–1286.
45 O. Z. Yesilel, G. Gunay and O. Buyukgungor, *Polyhedron*, 2011, **30**, 364–371.
46 C. S. Liu, P. Q. Chen, Z. Chany, J. J. Wang, L. F. Yan, H. W. Sun, X. H. Bu, Z. Y. Lin, Z. M. Li and S. R. Batten, *Inorg. Chem. Commun.*, 2008, **11**, 159–163.
47 T. W. Hambley, *Inorg. Chem.*, 1998, **37**, 3767–3774.
48 H. V. Huynh, Y. Han, J. H. H. Ho and G. K. Tan, *Organometallics*, 2006, **25**, 3267–3274.
49 D. Sun, N. Zhang, Q. J. Xu, R. B. Huang and L. S. Zheng, *J. Organomet. Chem.*, 2010, **695**, 1598–1602.
50 P. G. Jones, O. Crespo, M. C. Gimeno and A. Laguna, *Acta Crystallogr., Sect. C: Cryst. Struct. Commun.*, 2006, **62**, M411–M412.
51 R. Ghiasi and M. Monnajemi, *J. Korean Chem. Soc.*, 2006, **50**, 281–291.
52 C. F. Yan, L. Chen, R. Feng, F. L. Jiang and M. C. Hong, *CrystEngComm*, 2009, **11**, 2529–2535.
53 D. Frenkel and B. Smit, *Understanding Molecular Simulation: From Algorithms to Applications*, Academic Press, San Diego, 2002.
54 A. I. Skoulidas and D. S. Sholl, *J. Phys. Chem. A*, 2003, **107**, 10132–10141.
55 T. Premkumar and S. Govindarajan, *World J. Microbiol. Biotechnol.*, 2005, **21**, 479–480.
56 T. Premkumar and S. Govindarajan, *World J. Microbiol. Biotechnol.*, 2006, **22**, 1105–1108.
57 O. Zimhony, C. Vilcheze, M. Arai, J. T. Welch and W. R. Jacobs, *Antimicrob. Agents Ch.*, 2007, **51**, 752–754.
58 O. Z. Yesilel, G. Kastas, C. Darcan, I. Ilker, H. Pasaoglu and O. Buyukgungor, *Inorg. Chim. Acta*, 2010, **363**, 1849–1858.
59 S. Silver and L. T. Phung, *Annu. Rev. Microbiol.*, 1996, **50**, 753–789.
60 P. Dibrov, J. Dzioba, K. K. Gosink and C. C. Hase, *Antimicrob. Agents Ch.*, 2002, **46**, 2668–2670.
61 M. Rai, A. Yadav and A. Gade, *Biotechnol. Adv.*, 2009, **27**, 76–83.
62 B. S. Atiyeh, M. Costagliola, S. N. Hayek and S. A. Dibo, *Burns*, 2007, **33**, 139–148.
63 F. J. Liu, D. Sun, H.-J. Hao, R.-B. Huang and L.-S. Zheng, *CrystEngComm*, 2012, **14**, 370–382.